Eidgenössische Technische Hochschule Zürich
Swiss Federal Institute of Technology Zurich

Sideband locking for cavity bulk optomechanics

Semester Thesis

Javier Naya Hernandez
javier.naya.hdez@gmail.com

Laboratory for Solid State Physics
Departement of Physics, D-PHYS
ETH Zürich

Supervisors:
Tom Schatteburg
Yiwen Chu

January 27, 2022

Abstract

Cavity bulk optomechanics experiments require the use of two optical resonances with a free spectral range equal to that of the Brillouin frequency of a crystal. To keep the frequency of a laser at resonance a Pound-Drever-Hall control loop is used, which requires a signal of light reflected from the cavity. In case of an experiment that would use light pulses to coherently manipulate the optomechanical degrees of freedom, the reflected signal may not be sufficient to maintain the frequency stabilization feedback loop. In this work we propose the use of a third frequency, generated via intensity modulation and tuned to a cavity mode, to stabilize the frequency without interacting with the optomechanical experiment. We delve into the noise sensitivity of the mode structure of such cavity in order to explore the viability of our design, and construct a proof of concept experiment by doing measurements on a free-space Fabry-Perot cavity and a cavity containing a crystal for optomechanical coupling.

Contents

Chapter 1

Introduction

We have transitioned from the abstract mathematics of quantum mechanics to pursuing more and more complex implementations of these systems in labs around the world. While quantum mechanics has a rigid structure of Hilbert spaces and states, translating that to the language of experimental physicist it can mean working with atoms, ions, superconducting circuits, nitrogen vacancies, and many other creative implementations. Each platform has varied technical and scientific advantages and limitations, but also offer exciting opportunities for progress in the field. One such novel approach is the use of vibrations of a crystal that can interact coherently with light [1], by placing it inside an optical cavity such that for some optical modes their frequency difference is equal to a crystal dependent constant known as the Brillouin frequency.

In order to shine light inside the cavity at the desired frequencies we need to protect the system against undesired noise of both the cavity or the laser, for that a common and useful technique is the Pound-Drever-Hall frequency stabilization (PDH) [2]. The PDH technique works by modulating the phase of the incoming laser beam and mixing the reflected cavity light with the same local oscillator to create an error signal that is linear around the cavity resonances, and thus can be stabilized using a standard control loop. While there are subtleties to the PDH technique, for our purposes if we observe an error signal similar to the one in 1.1, then it's possible to stabilize the frequency in our experiment.

In a typical bulk optomechanics experiment the laser is locked into one of the two modes separated by the Brillouin frequency, and then a sideband with the desired frequency spacing is generated using an Intensity Modulator (IM). But in the case we desire a coherent control of the vibrational modes it will be necessary to use pulses of light instead of a continuous beam. However if there is no reflected signal then there is no PDH error signal,nd noise in the system can cause the laser frequency to shift out of resonance.

To offer a possible solution to the pulsed operation problem we investigate the viability of performing the laser locking with a third mode of the cavity that does not participate in the optomechanical interaction, and it's then not affected by the pulsing of the two modes separated by the Brillouin frequency. This third mode is generated with an intensity modulator, so it will be a sideband to the carrier frequency. We will refer to this process as sideband locking. The goal of this report is to test whether we can lock the laser frequency using a sideband, if we can have the carrier frequency stay on resonance after locking to the sideband, and to test how reliable sideband locking is by testing it on a Fabry-Perot cavity and the optomechanical cavity with a crystal inside.

This report is divided into a simulation and experimental portion. The simulation

section presents the Free Spectral Range (FSR) spectrum of the optomechanical cavity, which we use it to study the sensitivity of different mode pairs with respect to changes in the cavity length. This provides information about which sets of mode pairs frequency differences are less susceptible to cavity length noise, which we refer to as displacement insensitive modes. The experimental section describes the optical setup and procedure used to achieve sideband locking, and results from experiments in a standard Fabry-Perot cavity and the previously described optomechanical cavity.

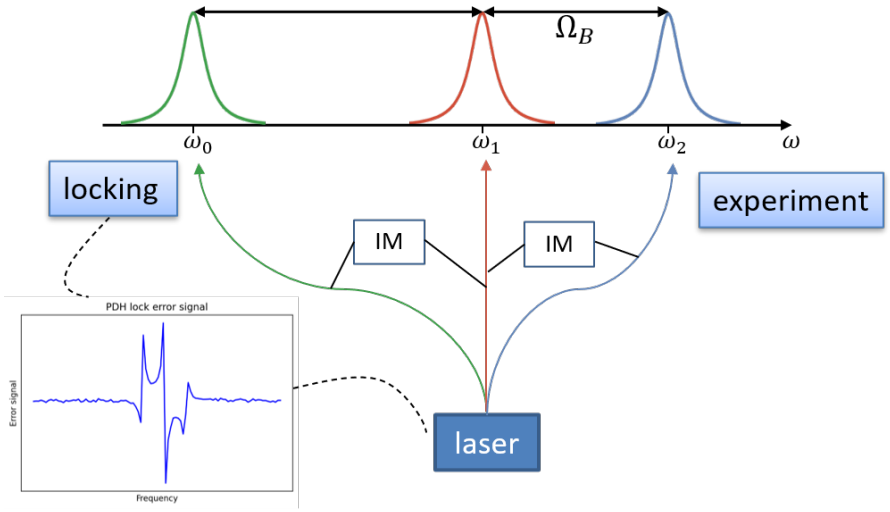

Figure 1.1: Scheme proposal for using sideband locking in the bulk optomechanics experiment. Here Ω_B represents the Brillouin frequency. Laser frequency is locked to the cavity mode ω_0 via the PDH error signal, and the ω_1 and ω_2 modes are used for the optomechanical experiment. Different mode frequencies are generated with intensity modulators

Chapter 2

Simulations

2.1 Cavity Transmission Spectrum

A Fabry-Perot cavity is one of the most commonly used optical resonators, consisting of two mirrors facing each other at a distance L and, in our case surrounded by vacuum (or air) between them. A relevant property of the cavity is the frequency difference between two adjacent modes, called the Free Spectral Range (FSR) and defined as

$$FSR_i = \nu_i - \nu_{i-1} = \frac{c}{2L}, \tag{2.1}$$

with c being the speed of light. For this simple case the FSR is constant across all different modes of the cavity.

In the case of the bulk optomechanical experiment, the quartz crystal inside the Fabry-Perot modifies the uniform FSR spectra of the Fabry-Perot, thanks to reflections at the faces of the crystal as can be seen in figure 2.1.

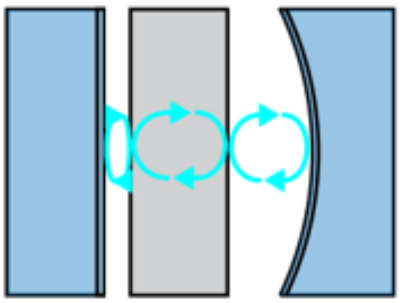

Figure 2.1: Cavity used for the optomechanical experiment. Arrows represent reflections on the edges of the crystal Figure taken from [1].

To find the index of refraction we follow the procedure outlined in the supplementary material of reference [1], where the transmission matrix method is used. Taking into account all of the reflections and propagation inside of the system the final transmission matrix is of the form

$$\begin{aligned}\mathcal{T} =& \frac{-i}{t_1}\begin{pmatrix}-1 & r_1\\ -r_1 & 1\end{pmatrix}\cdot\begin{pmatrix}e^{i\omega d/c} & 0\\ 0 & e^{-i\omega d/c}\end{pmatrix}\cdot\frac{-i}{t_0}\begin{pmatrix}-1 & r_0\\ -r_0 & 1\end{pmatrix}\cdot\\ &\begin{pmatrix}e^{i\omega L_{quartz}/c} & 0\\ 0 & e^{-i\omega L_{quartz}/c}\end{pmatrix}\cdot\frac{-i}{t_0}\begin{pmatrix}-1 & -r_0\\ r_0 & 1\end{pmatrix}\cdot\\ &\begin{pmatrix}e^{i\omega(L-L_{quartz}-d)/c} & 0\\ 0 & e^{-i\omega(L-L_{quartz}-d)/c}\end{pmatrix}\cdot\frac{-i}{t_2}\begin{pmatrix}-1 & r_2\\ -r_2 & 1\end{pmatrix}\end{aligned} \tag{2.2}$$

and the reflection power spectrum can be found with $P_r = \left|\frac{\mathcal{T}_{1,2}}{\mathcal{T}_{2,2}}\right|^2 P_{in}$, with P_{in} being the input power. It's possible to analytically find the reflection spectrum but the expression results too cumbersome and complicated to be worth it. The simulations were performed using a python code developed internally by Tom Schatteburg, the output of which contains an array of the mode resonances for a given set of parameters by performing the matrix multiplications from equation 2.2.

In figure 2.2 an example FSR spectrum is shown in blue points, the apparent oscillations are a consequence of the crystal surfaces passing through the nodes and anti-nodes of the standing wave optical cavity modes.

Choosing parameter values would change the shape of the FSR spectrum, in the case of very small perturbations of cavity length the mode frequencies shifts slightly, and the FSR of the corresponding mode also changing as a result. To understand the trajectory the FSR spectrum the figure 2.2 presents a sweep of the cavity length by about 1 μm with very fine steps. As a results the possible values the FSR spectrum can take are more apparent, with clearly defined maximums and minimums that are usually not reached for a given set of cavity parameters.

The periodic nature of the FSR spectrum is due to oscillations in the supported modes whenever the cavity length is changes. As observed in figure 2.3 the frequency of the modes does decrease whenever L is increased, as expected given larger wavelengths are allowed in the cavity. But each mode presents small oscillations on top of the linear behaviour.

2.2 Displacement Insensitive Modes

The system under consideration is particularly sensitive to vibrational noise given it is placed inside a dilution fridge and not isolated on top an optical table. The experiment relies on a particular mode pair having an FSR of Ω_B, and we know from the previous section that the FSR fluctuates with respect to cavity size changes, therefore choosing a pair of modes that are less susceptible to vibrations is a good strategy to obtain clean experimental results. This behaviour has been previously observed when Optomechanically Induced Transparency and Amplification (OMIT/A) experiments were performed, choosing different pairs of modes yielded better or worse results depending on their positions relative to the FSR spectrum.

Considering the set of three modes proposed for the sideband locking scheme, we

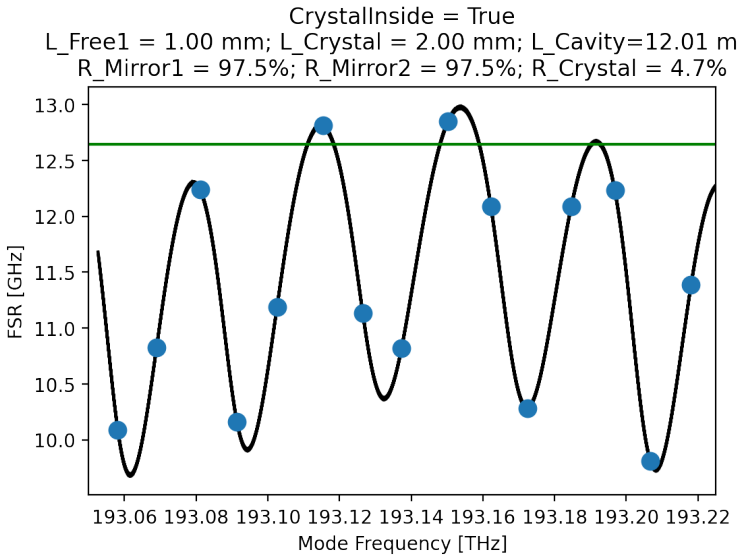

Figure 2.2: Simulated FSR spectrum of the optomechanical cavity. Cavity parameters given in the figure, the crystal index of refraction is set to $n = 1.55$. A fine 1 μm cavity length sweep is plotted in black to showcase the oscillatory nature of the FSR. Blue points represent the usual cavity spectrum encountered for a fixed set of parameters. The green line represents the Brillouin frequency of $\Omega_B = 12.645$ GHz taken from [1].

require two pairs of modes which simultaneously fulfill the displacement insensitive condition of $\frac{\partial FSR}{\partial L} = 0$ for a specific cavity length. The experimental justification being that while the PDH lock corrects for the noise of the locked cavity mode, noise from the second mode shifts the FSR away from the Brillouin frequency.

To search for displacement insensitive pairs of modes we not only look at adjacent modes but also ones that are further apart, we still keep using the terminology of FSR but refer to frequency differences of arbitrary pairs of modes, focusing mostly on pairs with one or two other modes in between them. On figure 2.4 we can observe the generalized distance for different pairs of modes for different cavity lengths. Notice consecutive pairs (19-20,20-21) present the same periodic behaviour but with a phase difference, the same as for pairs (18-20,20-22). Modes of distance three (23-20,17-20) apart don't exhibit the same oscillations as the rest of the pairs, this behaviour appears to be more or less general and repeats itself over simulations with different parameters and focusing on different sets of modes, but given the complicated nature of the analytical expression it would be difficult to call this a general result.

Figure 2.5 plots the changes in FSR for different mode pairs. This is where the sensitivity of the system is more noticeable. There are some configurations where mode pairs can have changes of a few MHz for only a nm in cavity length noise, which is about the Full Width Half Maximum (FWHM) of the optical resonances in the cavity. The maxi-

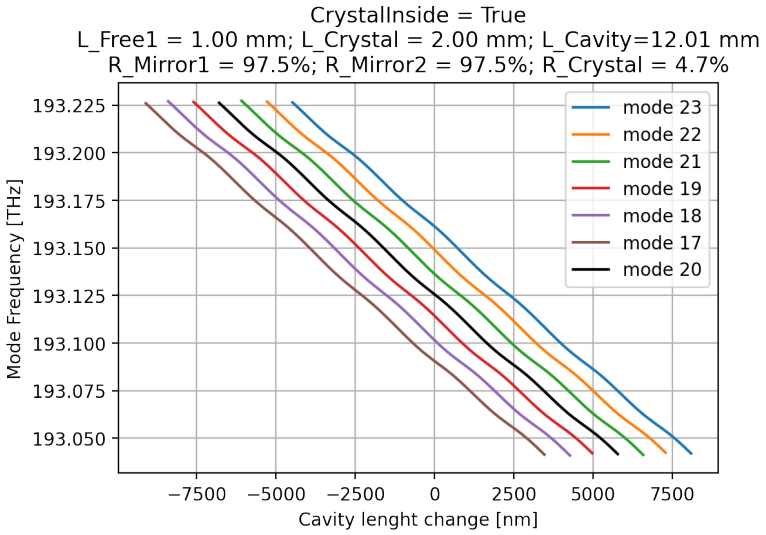

Figure 2.3: Change of the mode frequency with respect to changes in the cavity length. The expected decrease in frequency for a free space cavity is evident, but also visible are small oscillation due to the presence of the crystal

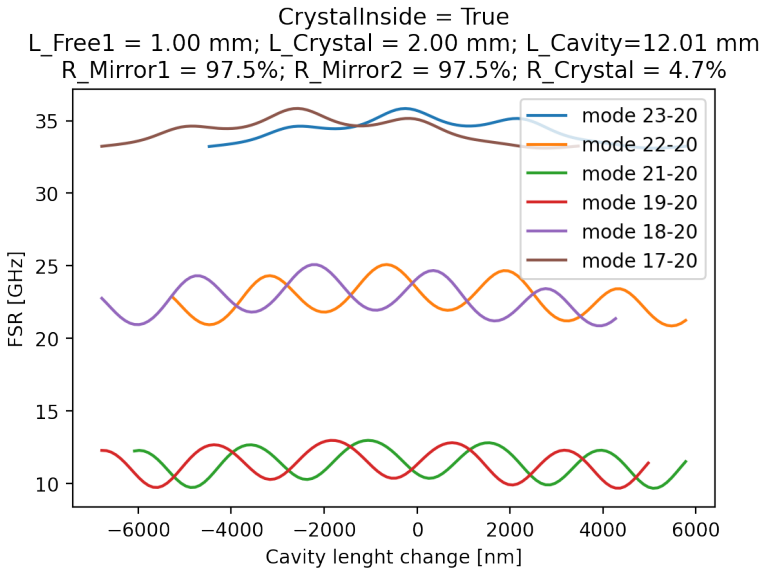

Figure 2.4: Absolute distance between different pairs of modes for different cavity displacements. The commonly defined FSR ($f_j - f_{j-1}$) corresponds to the red curve. Due to oscillations present in the modes, as seen in figure 2.3, their distances also have an oscillatory behaviour.

mum amplitude of the derivatives seems to be roughly the same regardless of which pairs of modes is compared (except for the modes distance three apart) but there is a phase difference for each one. From this figure we can observe that whenever there is a length value for which a mode pair is displacement insensitive, it's not always possible to find another one that is also crossing the zero line. But in some cases there are two pairs that are displacement insensitive for a given cavity length, specifically in the interval between -4000 nm and -3000 nm there is a point where both mode pairs 20-21 and 20-18 are displacement insensitive simultaneously, the same for the pairs 20-22 and 20-19. It could be the case that there are further pairs of modes for which this condition is fulfilled but their frequency differences would be of more than approximately 40 GHz, which is not feasible to achieve with intensity modulators.

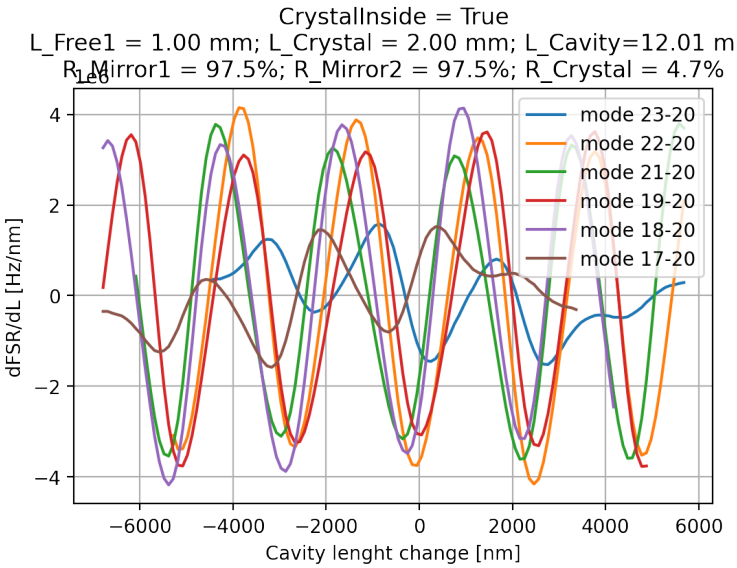

Figure 2.5: Derivative of the general FSR (distances between arbitrary different set of modes) with respect to cavity displacements. Data is the same one as in figure 2.4. Displacement insensitive points correspond to positions for when $\frac{dFSR}{dL} = 0$. The units in the y-axis should read $[MHz/nm]$

To facilitate visualization of the previous results we map the displacement insensitive points onto the FSR spectrum of mode 20 in particular. That is, whenever the FSR change crosses through zero in figure 2.5 we extract the respective cavity length and plot the FSR of mode 20 ($f_{20} - f_{19}$) at that particular cavity length. The reason for this being that during the lab experiments the FSR spectrum is the information available to us, and being able to identify whether the modes pairs observed are displacement insensitive or not is of great convenience. In figure 2.6, we can observe this mapping. Focusing first on the displacement insensitive points for the mode pair 19-20 (FSR of mode 20), as a sanity check we can see it's displacement insensitive at the top and bottom of the black curve of possible values for the FSR. This is expected from the expression

$$\frac{\partial FSR}{\partial L} = \frac{\partial FSR}{\partial f} \cdot \frac{\partial f}{\partial L} \tag{2.3}$$

so given $\frac{\partial f}{\partial L} \neq 0$ then a displacement insensitive point for the mode pair 19-20 is also a point where $\frac{\partial FSR_{20}}{\partial f} = 0$, so at the top and bottom of the oscillation.

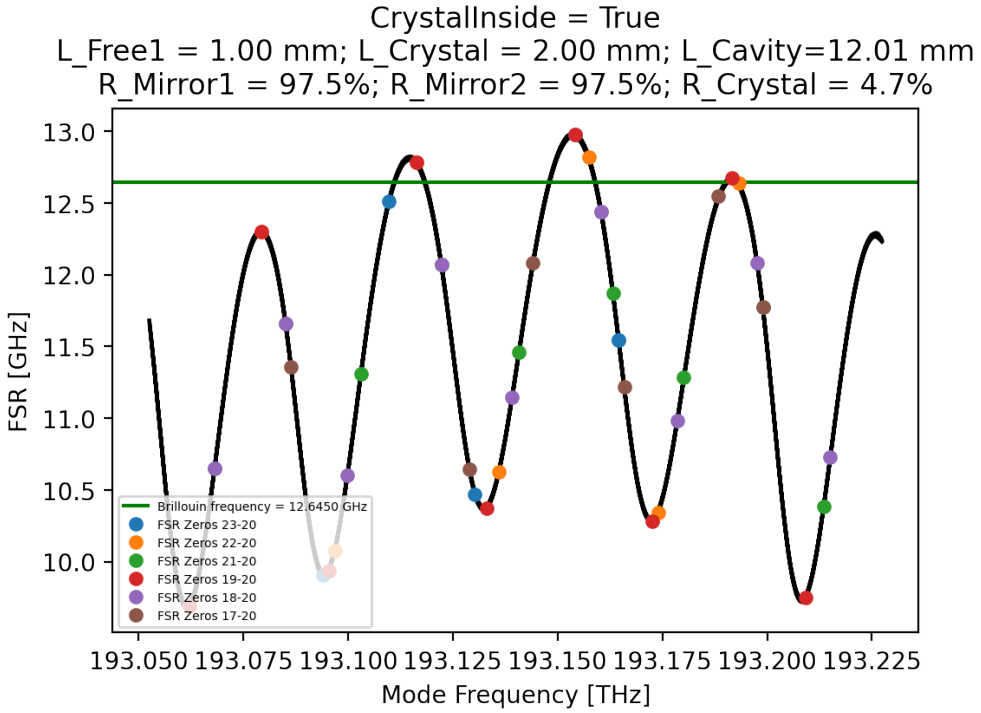

Figure 2.6: Mapping of the displacement insensitive points from figure 2.5 onto the FSR spectrum of mode 20. Notice the positions where the red ($f_{20} - f_{19}$ displacement insensitive) and orange points agree ($f_{22} - f_{20}$ displacement insensitive). This corresponds to a group of three displacement insensitive points.

Also of relevance are the mode pairs 20-21, where thanks to the phase difference observed in figure 2.4 the displacement insensitive points are in the middle of the oscillations, so it's not possible to find three consecutive modes where their frequency differences are displacement insensitive. As for the mode pair 20-22 the displacement insensitive points seem to coincide with the displacement insensitive points for the mode pair 20-19 for some frequencies, a pattern which was again observed to be consistent regardless of the modes chosen or the cavity parameters. For example if choosing to plot the FSR of mode 19 then the displacement insensitive points at the top and the bottom of the oscillations would be the pairs 18-19 and 19-21.

Although we cannot conclude our observations to be general for every case, we have found convincing evidence that pairs of modes $(j,j \pm 1)$ and $(j \mp 2,j)$ to be potential

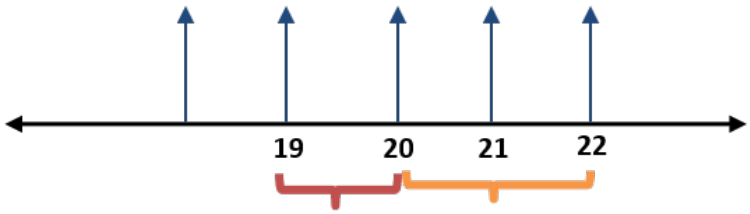

Figure 2.7: Visual representation of the group of three displacement insensitive points from figure 2.6. This property seems to be general to modes other than the ones presented above, that is, pairs $(j,j \pm 1)$ and $(j \mp 2,j)$.

candidates for the proposed sideband locking scheme.

Chapter 3

Experiments

3.1 Experimental Setup

For the experimental section we focused on providing a proof of concept for the sideband locking scheme by working with only two modes. The goal being to lock onto a sideband while still keeping the carrier on resonance, so in this case no optomechanical interaction. It will also be an important tool to test how stable the FSR of the cavity by studying how the cavity noise levels displace the carrier off resonance.

The setup used to generate these two different modes is shown in figure **??**. The laser light is split into two amrs via a 50/50 beam splitter, with one arm having only a Variable Optical Attenuator, and with the other one containing an IMP-1550-10-PM 10 GHz Intensity Modulator with an external RF signal produced by a Windfreak SynthHD 10 MHz - 15 GHz microwave generator whose signal is amplified by an iXblue DR-AN-20-MO as to obtain enough power to resolve the sidebands. This is followed by an MPZ-LN-10 Phase Modulator driven at around 32 MHz and 18 dB. Also not shown in the diagram is the PDH locking scheme connected to the phase modulator to create the error signal, for simplificity purposes we can assume that signals that pass through the phase modulator are the ones that can create a PDH signal. After the phase modulator we include a filter that we use to filter out the carrier frequency of the IM and keep only the sideband signal, the filter used is the Ultra-Narrow Band-Pass Filter Module IXC-FBG-PS-M with a 4 GHz bandwidth, small enough to discriminate the sideband and tunable within a range of 1550 ± 0.1 nm. We label it as a Fiber Bragg Grating (FBG) due to it using a combination of two FBG to archive the desired filtering. The signal from both arms of the setup is recombined before being sent to the cavity, where a circulator is used to measure the reflected signal.

3.1.1 Frequency Sweeping

The laser used for these experiment is the TOPICA CTL-1550 with the DLC pro Digital Controller, which provides a quick and intuitive way to lock the laser frequency. We just need to supply it with a PDH error signal as we're able to lock onto the desired resonance. For this to happen the controller has an option to do a fast frequency sweep of a range around 50 GHz with frequencies of up to 100 Hz. This is the tool used to identify the PDH error signal and then lock to the respective resonance. Also included in the controller is an automatic locking scheme, we only need to supply the appropriate error signal and select the resonance.

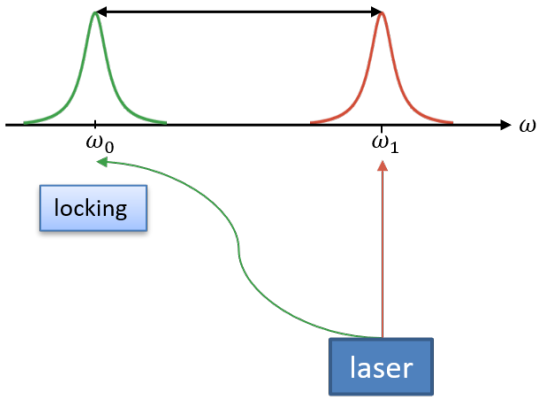

Figure 3.1: Modes uses for the experiments. Locking onto a sideband and pulsing at the other mode frequency, no third mode was used.

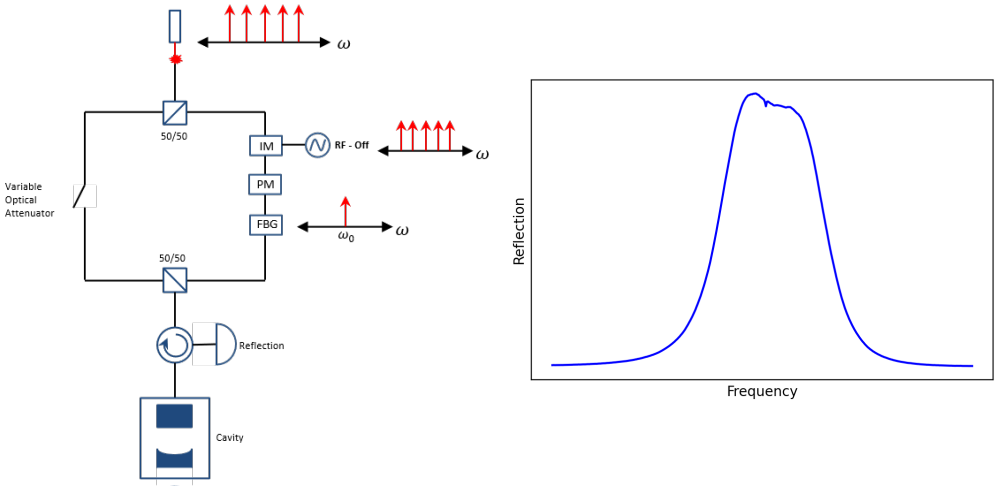

Figure 3.2: **a.** Simplified experimental setup used for the experiments. The laser is performing a frequency sweep over a range of 50 GHz with a frequency of 100 Hz. The phase modulator (PM) is driven at 32 MHz with 18 dB amplitude and is used to generate the PDH error signal for the locking. The FBG represent a narrow band pass filter with transmission frequency of ω_0. **b.** Reflection spectrum of the frequency sweep when the IM is not driven. Shape due to the narrow band pass filter having a bandwidth.

To make sense of the measured signals in the experiments we first focus on a simplified version without driving the intensity modulator, so light passing through it is only attenuated, with the DC bias voltage set to maximize transmission. The phase modulator information makes it possible to lock onto any resonance within the frequency sweep range, while the filter only transmits light around ω_0, which we tune to be a resonance

of the cavity. The experimentally measured reflection signal is shown in figure **??**, the cavity resonance is seen as a small dip around the center, but not well resolved enough due to the coarse sampling rate of the frequency sweep.

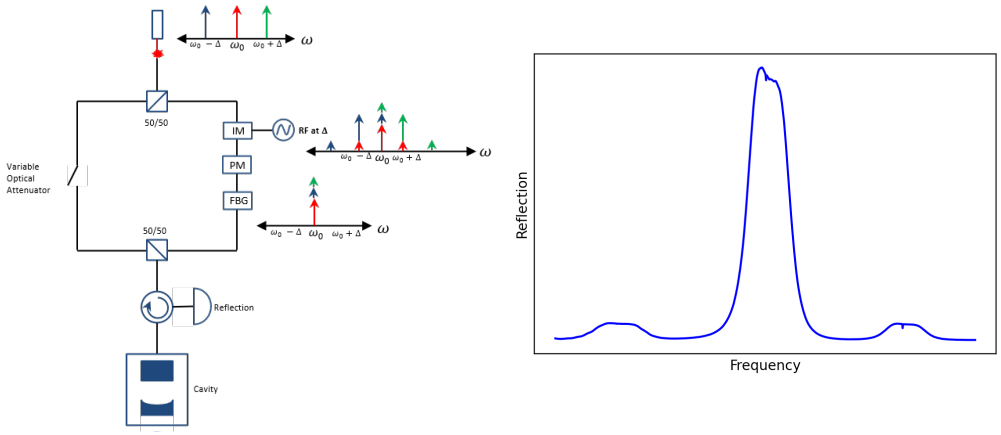

Figure 3.3: **a.** Same experimental setup as in figure **??** but with the IM being driven with frequency Δ. The frequency sweep parameters are kept the same. Light from the frequencies $\omega_0 \pm \Delta$ is transmitted through the filter due to the sidebands generated by the intensity modulator. **b.** Reflection spectrum of the frequency sweep when the IM is driven at frequency Δ. Resonances seen in both of the sidebands are light transmitted through the resonance at frequency ω_0.

In the case whenever we drive the intensity modulator with frequency Δ, light emitted at a frequency $\omega_0 - \Delta$ will have sidebands at $\omega_0 - 2\Delta$ and ω_0, the latter of which passes through the filter and is measured. Similarly for light at $\omega_0 + \Delta$. The resulting spectrum is shown in figure **??**. The resonances present in the sidebands corresponds to light at frequency ω_0 being reflected at the cavity and as such represent a mode at such frequency, event though the light is detected whenever the laser shines a light at frequencies $\omega_0 \pm \Delta$. The presence of a resonance in the spectrum sidebands creates a PDH error signal as seen in figure 3.4, allowing us to lock onto the carrier (frequency ω_0), or the sidebands (frequency $\omega_0 \pm \Delta$).

Although there is a resonance signal in the sidebands of figure **??**, the reflected intensity is too low to successfully lock onto the sideband. Several factor contributing to this are: the intensity modulator being rated at 10 GHz while we're driving at 12 GHz, the RF power provided directly by the generator can only provide 18 dB at our driving frequency while the maximum rated power for the IM is 25 dB, the DC bias voltage not being optimized to maximize sideband power and attenuation resulting from the optical components in the arm. The problem was solved by including an RF amplifier that increased the signal up to 21 dB and by tuning the DC bias voltage to a point where the sideband power was maximized. The resulting spectrum as shown in figure 3.5, and

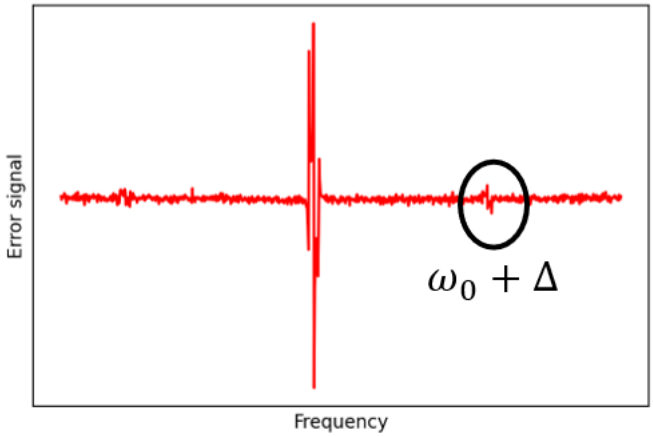

Figure 3.4: Error signal obtained from the reflected signal shown in figure **??**. Highlighted section corresponds to the PDH error signal generated from the sidebands.

provided good enough to perform the sideband locking experiments.

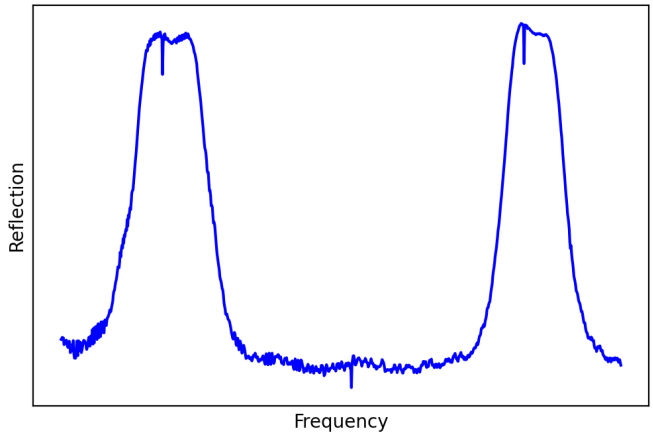

Figure 3.5: Reflection spectrum of the experimental setup described in figure **??** in the case of using an amplifier to increase the power of the RF signal used in the modulation and with optimal bias voltage in the IM. Higher reflected power on the sidebands mean a better signal for sideband locking.

3.1.2 Sideband Locking

Descriptions of the sideband locking scheme have so far not taken into account the second arm of the experiment which is controlled by a VOA. While the arm without the intensity modulator contains information about the resonance in ω_0 in the sidebands $\omega_0 \pm \Delta$, the second arm contains information about the standard cavity spectrum, showing

a resonance at ω_0 and, considering for the moment a free-space Fabry-Perot cavity, at $\omega_0 \pm FSR$. So if we know the cavity FSR, which is normally the case, we can set $\Delta \sim$ FSR. The frequency spectrum of such case is shown in figure 3.6, where the mode with the small sidebands is the light passing through the phase modulator.

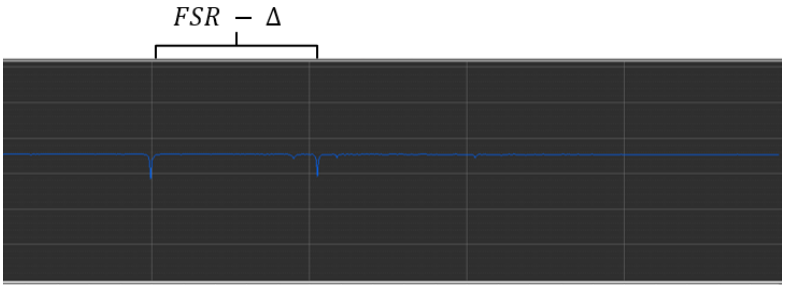

Figure 3.6: Reflection signal frequency spectrum close around the sidebands. The resonance dip with low frequency sidebands being the same as the ones from figure **??**, identifiable because the sidebands are created due to the phase modulator, and corresponding to the resonance at ω_0 of the cavity. The second dip coming from light passing through the second arm as seen in figure **??**

Locking the laser to one of the sidebands results in its frequency set to $\omega_0 + \Delta$, chosen without lack of generality. The light from the IM arm will contain a small sideband with frequency ω_0, which as previously mentioned is a resonance of the cavity, while the VOA arm will pass by without altering its frequency. Such that before entering the cavity there a superposition of both frequencies, one that is on resonance (ω_0) and another one that we can tune to be on resonance $\omega_0 + \Delta$. We can then use the tunability of our RF drive to sweep around the FSR of the cavity as a way to probe the cavity resonances, and by setting $\Delta =$ FSR we can have our desired sideband locking scheme with locking onto sideband while pulsing (arbitrarily varying the intensity) of a second frequency tone on resonance.

3.2 Free-Space Cavity

To provide an experimental proof of concept of the arrangement we first worked with a free-space Fabry-Perot cavity set on top of an optical table. The equally spaced modes and isolation from vibrational noise being ideal for this task. The FSR of the cavity being measured to be 12.9135 GHz. For the setup we use use the procedure described in figure 3.7 to lock onto the sideband. Once the laser frequency is set we only have access to time domain measurements of the cavity reflections and error signal. From here we can observe that changing the RF frequency in the range of a couple MHz either increases or decreases the average reflected signal. Taking 1 second measurements of every step and plotting the average reflected signal with its respective error bars reveals the shape of the resonances, as seen in figure **??**. The measurements were repeated for different reference

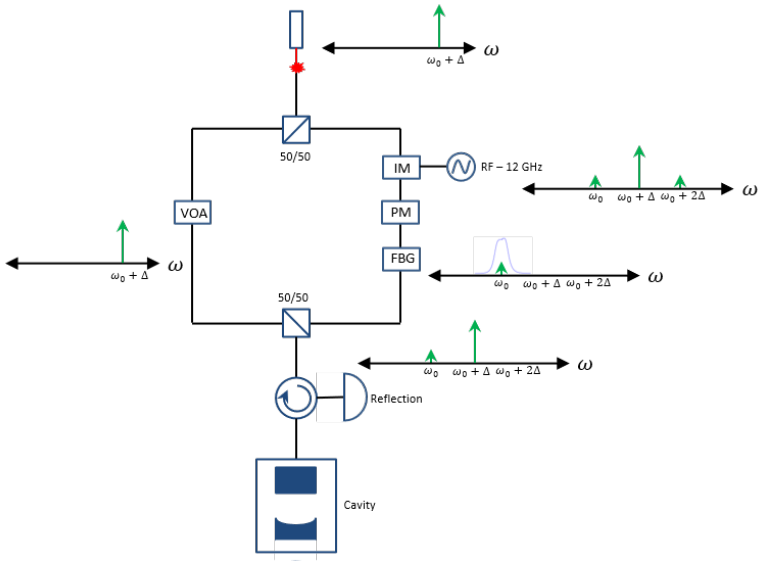

Figure 3.7: Frequency domain representation of the sideband locking experiments. The laser is locked to a sideband with the frequency $\omega_0 + \Delta$. After the 50/50 beam splitter the arm with the intensity modulator will create a sideband with the frequency ω_0 which will pass through the filter, while the other arm will only have an Variable Optical Attenuator (VOA). THe light from both arms are recombined before reaching the cavity. If Δ is tuned to the FSR of the cavity then both tones of light will be resonances.

powers (power measured after a 90/10 beam splitter before light reaches the cavity) and we can observe the expected increase of measured reflected signal, while on resonance the measured reflected light stays roughly the same for different powers. In the case of the VOA completely closing off the left arm of the setup (-24.6 dBm) and only light at ω_0 entering the cavity, we see a constant reflected value for different RF frequencies, which is expected given the light shined onto the cavity doesn't have information about Δ.

The error signals shown in figure **??** seem to have a constant pattern independent of the reference power measured. This is expected because the light intensity on the arm passing through the phase modulator is constant and independent on the intensity of the other arm. This means we can vary the intensity of the pulsing arm and not affect the locking, we could in theory turn off the pulsing arm for an arbitrary amount of time and the frequency would remain stable because of the locking using the second arm, which proves we can indeed successfully perform sideband locking.

Noise in this experimental setup can arise either due to fluctuations on the locking frequency (any non-zero error signal indicates deviations from the cavity resonance) or changes in the cavity FSR which leads to the $\omega_0 + \Delta$ being shifted off resonance. While the PDH lock is a robust method for stabilizing laser, frequencies changes in cavity frequencies also lead to changes in the FSR, so both noises are generally correlated. To

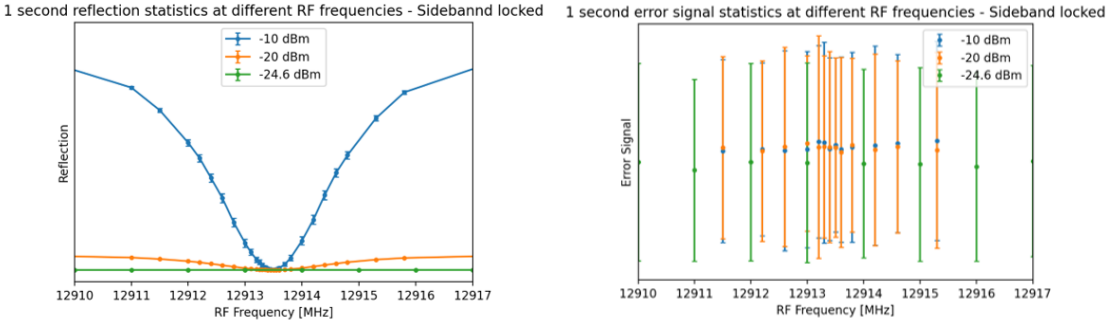

Figure 3.8: **a.** Average intensity with error bars of one second time traces of the sideband locking scheme presented in 3.7, with different Δ values and at different optical powers obtained by tuning the VOA. **b.** Error signal statistics for the data in figure **??**. Both averages and error bars remain constant for different optical powers, which is consistent with the error signal being encoded in the sidebands created by the Phase Modulator (PM), and that arm having a constant optical power across the different experiments.

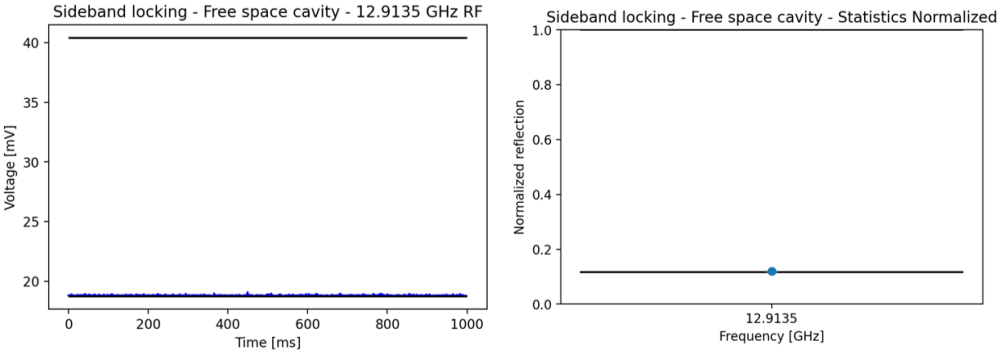

Figure 3.9: **a.** Time trace signal for the RF reflection signal tuned to $\Delta = FSR = 12.9135$ GHz, that is both modes on resonance. The top black bar represents the average signal whenever the $\omega_0 + \Delta$ mode is off resonance, and the lower one is the minimum value of the plotted signal. **b.** Normalized statistics of the time trace signal. Subtracting the white noise from the detector and treating the upper black line in figure **??** as one. Also the average measure reflectance is plotted alongside its error bars.

quantify the effect of such noise we use the time domain fluctuations of the reflected cavity signal. If there are any noises processes slower than the detector sampling rate (a few kHz) and faster than the measuring time (1 Hz), then the average reflected value of the one second measurement will be larger than the minimum measured reflectance

within that time period. In this way, a noisy locking would cause a shift off resonance of our light frequencies and show a larger standard deviation.

As we can see from the time traced signal in figure **??**, the signal stayed close to the resonance during the whole measurement process. To accurately compare different results later on we also present the statistics (mean and standard deviation) normalized to the detector value when Δ is far off resonance from the FSR and taking into account the detector white noise. So in case of the free-space Fabry-Perot cavity we can conclude that the noise levels are low enough as to call this an effective sideband locking scheme.

3.3 Optomechanical Cavity

After testing the sideband locking scheme with the Fabry-Perot cavity we can proceed onto the optomechanical cavity previously described in the simulation section. The cavity in question is mounted inside a dilution fridge operated at a temperature of 4K, with a pulse tube compressing and expanding gaseous Helium to act as a heat exchanger. Given the comparatively complex FSR spectrum, we first require to choose which mode pairs we will be testing and calibrating the narrow band pass filter to be set in one of the two. Although the filter has proven useful in the proof of concept for the sideband locking, its limited by the tunability range available (1500 ± 0.1 nm), meaning it's not possible to reach every mode of the cavity. Figure 3.10 shows the labeling of the mode pairs to be used in the experiments as well as their FSR spectrum. The goal is to prove the viability of the sideband locking scheme for the optomechanical experiment, and to test the claims about displacement insensitive modes from the simulation section.

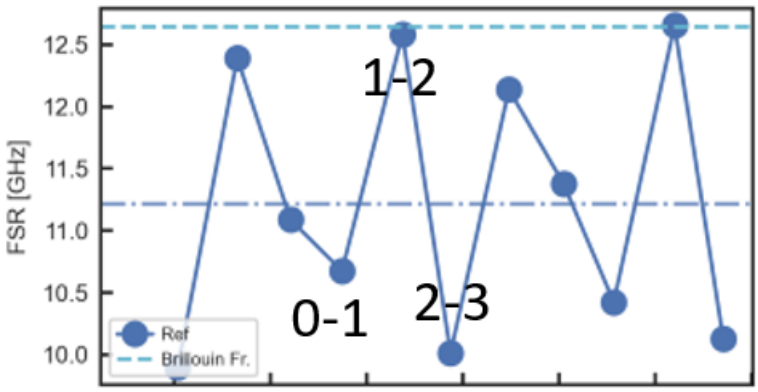

Figure 3.10: FSR spectrum of the cavity with the crystal and inside the dilution fridge. The numbered pairs of modes are the one the experiments were performed on. Note this spectrum changes when the cavity warms up.

To perform the experiments we require to turn off the pulse tube supplying the liquid helium, the vibrations it creates making it difficult to archive frequency locking. Once off, the temperature of the cavity increased around 2 degrees within 5 minutes, shifting the modes and the FSR spectrum in the process. Due to this problem we couldn't

reproduce the cavity mode shape like in figure **??**, but we can still manually look for a minimum reflection point with the RF set around the FSR of that particular pair. The strategy for finding the minimum turns out to be more complicated this time around, with noisier reflection signals and shifting FSR, for this reason we took several half a second measurements whenever the resonance point might have been found.

In figure 3.11 we found a collection of measurement results for the three different mode pairs, alongside their normalized statistics. For the mode pair 0-1 shown in 3.11a and 3.11b we took a 16 second long measurement at the same RF frequency which were then split into 32 measurements of half a second. As can be appreciated form the time trace measurements, the statistics remain relatively constant but quite noisy. The normalized statistics show how the oscillations present in the time domain measurements increase the average reflection, reaching up to halfway to the off resonance point. This was consistent with the hypothesised behaviour of the mode pairs 0-1 given it's not a displacement insensitive mode pair according to the results from figure 2.6, that is, it's not located at the top or bottom of the FSR spectrum oscillations.

The measurements for the mode pairs 1-2 (3.11c and 3.11d) still show the same oscillatory behaviour as the mode pair 0-1, but as the normalized statistics go it was possible to find an RF frequency for which the average intensity closer to the minimum reflected value. The same can be said about the mode pair 2-3 (3.11e and 3.11f). The measurements for this mode pair also show the FSR shift occurring due the heating of the cavity and the crystal, where three measurements were made at the RF frequency of 9.9829 GHz at different times and from the normalized statistics we can observe how the FSR shifts the laser out of resonance.

Both mode pairs 1-2 and 2-3 are shown to be more displacement insensitive than the 0-1 mode, as expected given they are closer to the top and bottom of the oscillations. But a conclusion from figure 2.6 was also that for a given displacement insensitive pair, the FSR for the next pair was highly sensitive. An explanation for this is that neither pairs 1-2 and 2-3 are fully displacement insensitive, recall that not all points in the FSR spectrum reach the local maximum permitted by small displacement on the cavity. In figure 2.2 for example, the FSR point at around 193.11 THz is displacement insensitive, while the point before and after that one are highly sensitive, while for the points around 193.14 and 193.15 THz both are consecutive and while close to the local maximum and minimum of the black curve neither one is fully displacement insensitive.

The Power Spectral Densities of the time domain measurements give us a greater insight into the noisy oscillations observable in all measurements. As seen for the second column of figure 3.12, all the measurements done have a significant peak at 8 and 16 Hz. These frequencies are relatively slow to arise from any electronics (the RF signals are in the order of MHz and GHz) and may arise due to the vibration isolation stage the cavity is set up on, consisting on a set of springs that the cavity hangs from. While the vibration isolation stage has been successful in reducing noise in the system it appears it has also given rise to either resonances or high transmission at low frequencies which compromise the stability of the cavity FSR. In conclusion turns out the sideband locking scheme has potential use as a sensor for the optomechanical noise, which is relevant in

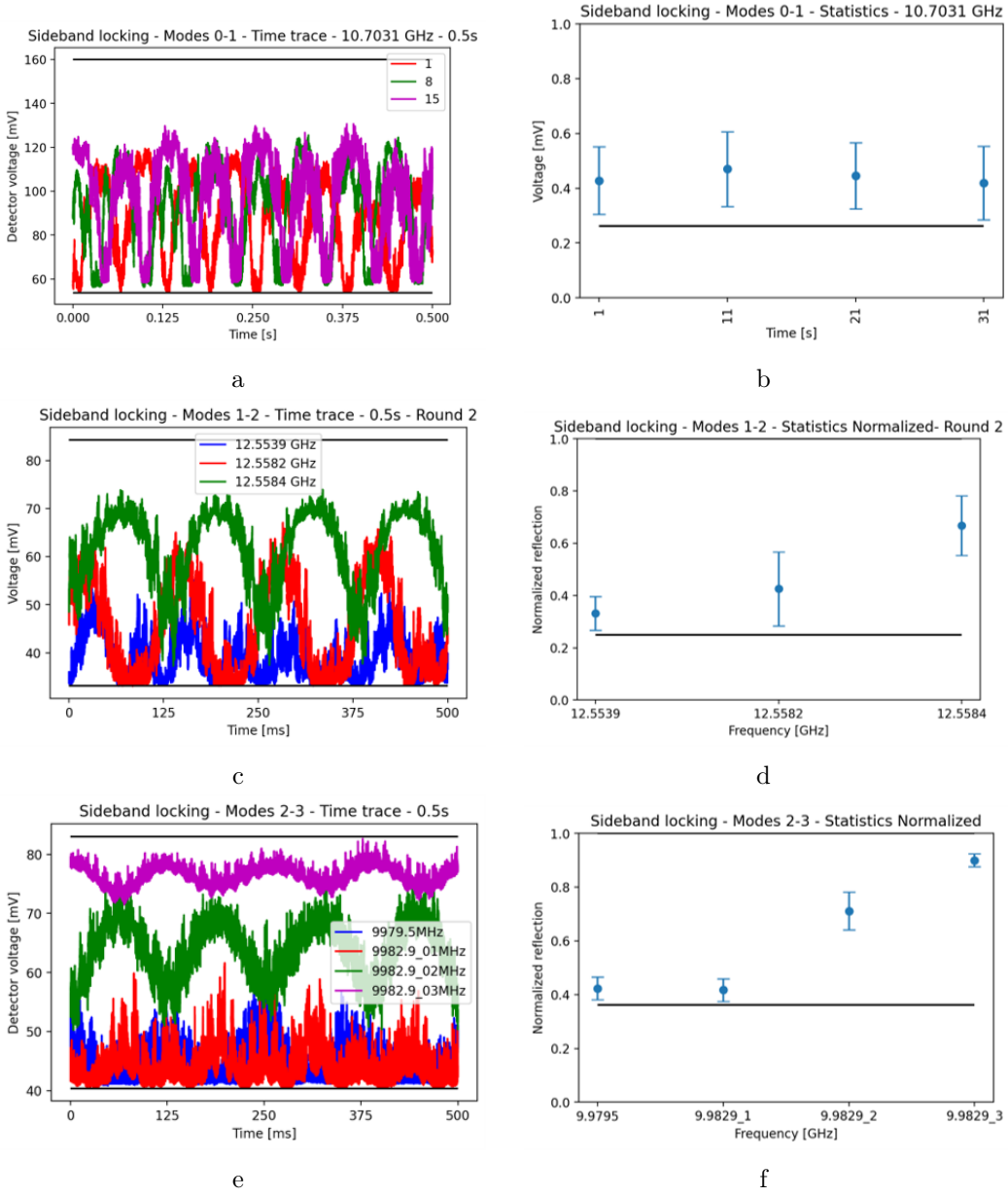

Figure 3.11: Sideband locking measurements performed with the scheme in figure 3.7 with the cryo cavity and with the pairs of modes specified in figure 3.10. The left column represents the time trace measurements at different RF modulation frequencies and at different times. The warming up the cavity slightly changes the mode frequencies making repeated measurements of the same point at different times potentially different. The right column contains information about the corresponding normalized statistics as presented in figure **??**.

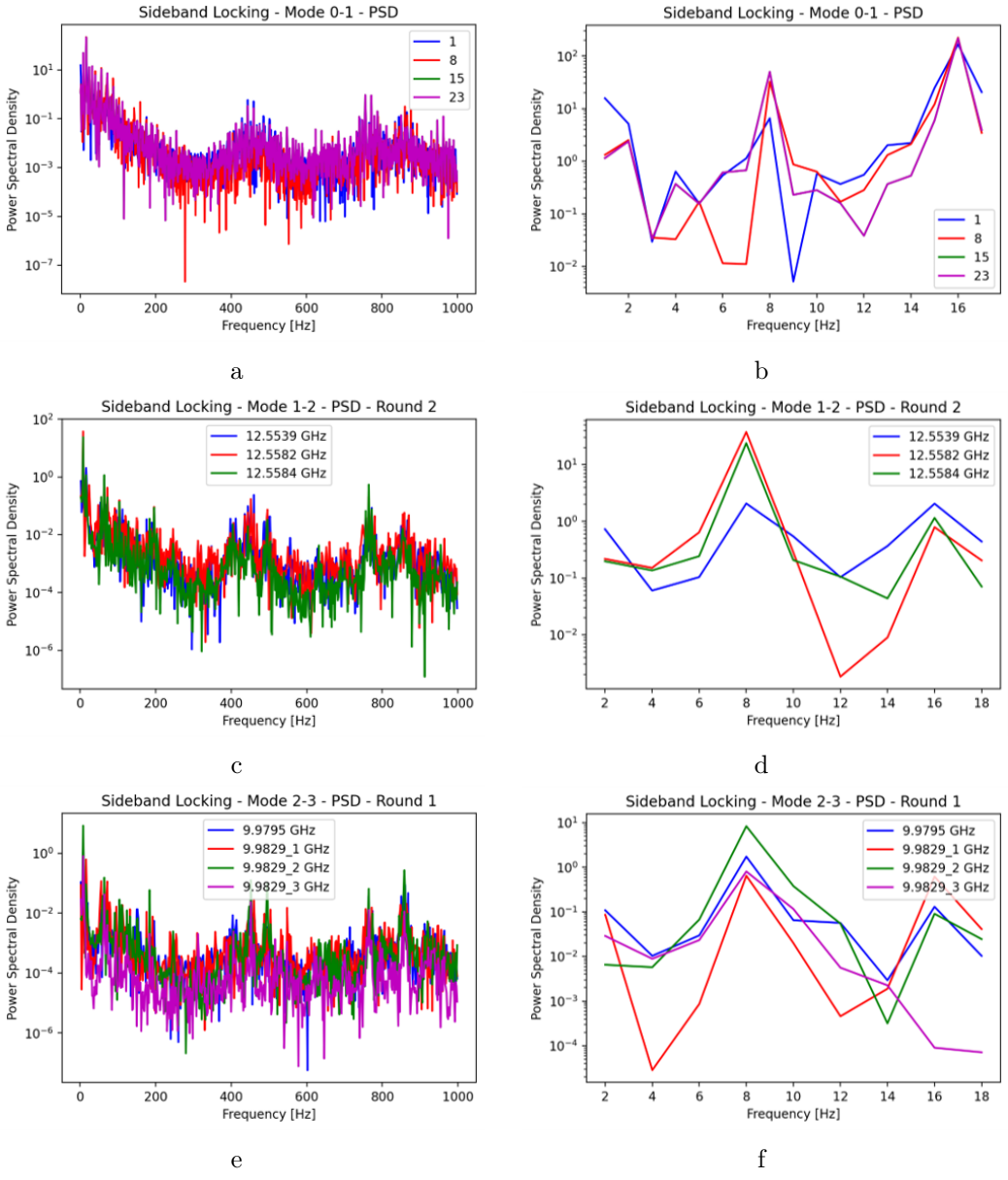

Figure 3.12: Power Spectral Density (PSD) of the time trace measurements from figure 3.11. The left column corresponds to the full spectrum available taking into account the detector sampling rate and the right column only shows a shorter slow frequency range where the highest peaks can be found. Prominent noise contributions at 8 and 16 Hz are present across all different measurements.

any kind of OMIT or thermometry experiment performed in it in the future.

Chapter 4

Conclusion

In this work we proposed a setup for stabilizing the laser frequency of a cavity bulk optomechanics by utilizing a third frequency tuned to a cavity mode generated by a in intensity modulator for the locking, which we call sideband locking. We studied the sensitivity of different pairs of modes to cavity length changes and found sets of three modes that are shown to be displacement insensitive and might be candidates for the proposed setup. We tested a proof of concept of the sideband locking scheme on a free-space Fabry-Perot cavity and in an optomechanical cavity inside a dilution fridge. We found evidence that supports our conclusion about displacement insensitive points in the optomechanical cavity and used the setup to obtain information about noise sources that affect the cavity.

While we showed that it's possible to perform sideband locking more works needs to be done in order to demonstrate whether it's a viable proposal for the pulsed experiment. No data was taken on the stability of modes that are further apart, for example how would the measurements for the pairs 1-3 be, which is an important part of the proposal. Also in the current state we don't have much flexibly to choose the modes we experiment with, due to the limited tuning range of the narrow band pass filter used, but the cavity length could be tuned in situ as to find ideal sets of displacement insensitive modes. Finding a way to suppress the 8 and 16 Hz noise could also give rise a much more stable sideband locking measurements and thus significantly improve the viability of the setup, given it requires not two but three modes maintaining their frequency distance with each other in order to work. There is also work to be done to setup a free-space detector to improve the signal to noise ration of the error signal and thus providing a more stable lock loop. Although there are still may open questions, we hope the work here serves as a stepping stone for further research and exploration of interesting phenomena related to FSR spectrums and optomechanical cavities.

Bibliography

1. Kharel, P. *et al.* High-frequency cavity optomechanics using bulk acoustic phonons. *Science Advances* **5.** ISSN: 23752548. arXiv: 1809.04020 (2019).
2. Black, E. D. An introduction to Pound–Drever–Hall laser frequency stabilization. *American Journal of Physics* **69,** 79–87. ISSN: 0002-9505 (2001).